EVALUATION OF UNCERTAINTY IN MUDWEIGHT WINDOW FROM ERROR PROPAGATION CONSIDERATIONS

Pierre Cerasi[1]

1: SINTEF Industry, pierre cerasi@sintef.no

Keywords: **drilling, automation, uncertainty, mud window**

RESUMEN

Evaluación de incertidumbre en la ventana de peso de lodo a partir de consideraciones de error de propagación.

En este trabajo, la propagación de errores es estimada en el modelo de la mecánica de rocas utilizado como parte de un nuevo simulador de perforación integrado y automatizado. El objetivo es una visualización simple de los límites de colapso y pérdida de lodo con sus incertidumbres asociadas, teniendo en cuenta la variación en el error del parámetro de entrada como una función de la posición en un campo y el origen de parámetro (correlación, pruebas de laboratorio, etc.).

El enfoque se basa en el cálculo de la matriz de covarianza para las incertidumbres en los esfuerzos de falla por estrés para los límites de presión en pozos (colapso y pérdida de lodo), en el base de coordenadas siguiendo el eje del pozo planeado. La matriz de covarianza se evalúa para diferentes modelos de fallas tales como Mohr-Coulomb, von Mises y Drucker-Prager. Las incertidumbres individuales de los parámetros de entrada son función de la distancia, tanto lateral como vertical. Estos puntos de calibración son pozos que penetran las mismas formaciones, donde hay datos de registros disponibles y/o se han realizado pruebas de pozo.

La incertidumbre total en la ventana de lodo estará gobernada fundamentalmente por los parámetros de entrada con mayor incertidumbre y los parámetros introducidos en funciones de mayor orden. Sin embargo, la calibración basada en el conocimiento previo o en características regionales como pozos existentes reducirán la incertidumbre de ciertos parámetros. Esto nos permite transmitir de manera simple a los ingenieros de perforación, el nivel de confianza en la ventana de peso de lodo pronosticado, sin tener que presentar en detalle las diferentes fuentes y los errores asociados en cada parámetro. Así, el ingeniero de perforación puede tener una advertencia previa sobre una mayor probabilidad de incidentes de perforación en los puntos donde la incertidumbre en la ventana de lodo es mayor. Esta incertidumbre también está evoluciona dinámicamente a medida que avanza la perforación, ya que la obtención de nuevos registros reducirá los errores al proporcionar un conocimiento más preciso sobre los cambios de litología, profundidad, porosidad y presión de poro. Aunque prácticamente ningún parámetro mecánico es directamente medido en la mayoría de las operaciones de perforación, especialmente en las formaciones arcillosas superiores, las correlaciones usadas con registros recientes obtenidos del pozo en progreso reducirán la incertidumbre comparada con lecturas similares en pozos cercanos.

La novedad de la aplicación de la propagación de error de cálculo del peso del lodo radica en la simple presentación visual, de inmediata importancia para el ingeniero de perforación. La naturaleza dinámica de la evolución de error durante la perforación, a medida que información más local (y por ende más confiable) es obtenida incrementalmente aporta a que el método sea atractivo.

INTRODUCTION

Rock mechanics considerations have taken a central role in drilling oil and gas wells, since the early 1980's (Bratli and Risnes 1981). It was recognized early on that the process of drilling wells resembles the engineering actions in boring tunnels, where attention has to be given to the risk of rock mass collapse and destabilization. Especially at depth, the presence of tectonic compressive stresses, with varying magnitude for all three principal components, makes it essential to be able to compensate for the missing rock matter excavated from the well as it progresses deeper Fjær et al. 2008). Redistribution of stresses around the borehole can only be counteracted with enough well pressure, through the use of a drilling fluid with sufficient density. When it comes to borehole stability on the way to the target hydrocarbon reservoir, most of the formations encountered on the way down are from the shaly lithology group, especially in the North Sea (Nes *et al.* 2012). Research efforts have thus naturally targeted shale and other low permeability formations, which essentially are expected to function as overburden and caprock anywhere trapped oil is hoped to be uncovered in subterranean reservoirs.

SINTEF Petroleum, now a part of SINTEF Industry, has been one of several groups dedicating continuous efforts to investigate the mechanical properties of shale formations (Nes *et al.* 2012). These efforts have spanned both laboratory experiments, carried out on field cores as available and representative outcrops, and theoretical and numerical modelling activities (Horsrud *et al.* 1998). Shales are complex rocks, with pore structure down to the nano-scale, permeability of the order of the nanoDarcy, anisotropic fabric with pronounced layering affecting mechanical, flow and acoustic properties and pronounced thermochemical attributes leading to mechanical impact as a function of the fluid in contact with the rock (Torsaeter *et al.* 2012). When drilling through shale formations, the drilling engineer may experience either mud losses, differential drillstring sticking, cavings production or wholescale borehole collapse (Lavrov and Tronvoll 2006). This can be compensated for by choosing a drilling fluid having not only the correct density, so as to provide enough support to the borehole wall by a sufficient well fluid pressure, but also the correct ion content in the form of dissolved salts (Fjær *et al.* 2002). These salt ions will interact with the near-well shale formations through osmosis and ion exchange mechanisms, leading to swelling or shrinkage of the shale, as the clay interlayers accommodate the inflow or outflow of ions (Karaborni *et al.* 1996). Straining of the shale is reflected in changes in stress conditions, which again may affect mechanical stability. Similarly, temperature gradients may translate to build-up of thermal stresses, if the formation cannot accommodate the expansion or contraction caused by the temperature changes quickly or freely enough (Lavrov and Cerasi 2013, Cerasi *et al.* 2014).

One of the results of many years with shale research at SINTEF has been the elaboration of an analytical borehole stability prediction tool, created by E. Fjær and more recently further developed by I. Larsen (Nes *et al.* 2013). Being the deliverable of a joint industry project running in consecutive 3-year phases, the software is a research tool continually under development, as new results are obtained and ever new refinements to the theoretical model are made. This tool is therefore not commercially available but used in-house, for wellbore stability studies. The main output of the software is a recommended mud weight window for drilling through shale layers, based on an input well path. The software calculates the state of stress on the planned borehole wall, by rotating the in-situ stress tensor to the axisymmetric coordinate system defined by the local borehole orientation (Fjær et al. 2008). It then examines the fulfilment or not of a chosen failure criterion, piecewise around the borehole in order to estimate whether shear or tensile failure could occur. This is repeated for all the input depths of interest. The user can choose from several failure criteria: Mohr-Coulomb, Drucker-Prager, modified Lade, etc. The tool also takes into account plasticity by correcting when examining the stress state by a factor called the plastic strain index; this index increases the linear strain at maximum shear stress defining the rock's strength by comparison with the calculated linear elastic strain. It is based on calibration against many triaxial tests on shale cores.

Other features of the software are the inclusion of a weak plane model, chemical strain based on osmosis, a semi-permeable membrane model, chemical activity of the drilling fluid and ion exchange mechanisms (Horsrud e*t al.* 1998, Lomba *et al.* 2000). These are based on laboratory fluid exposure tests, by which shrinkage and swelling as a function of stress state are predicted. On top of all this comes the calculation of thermal stresses, based on thermal contrast between well and rock temperatures (Torsæter and Cerasi 2015). The software allows the user to explore stability at a given depth, based on laboratory core test input including mechanical testing and fluid exposure testing. All input parameters are typed in in dedicated menus, for rock properties, stress state, choice of drilling fluids, thermochemical parameters etc. Another input mode is from prepared

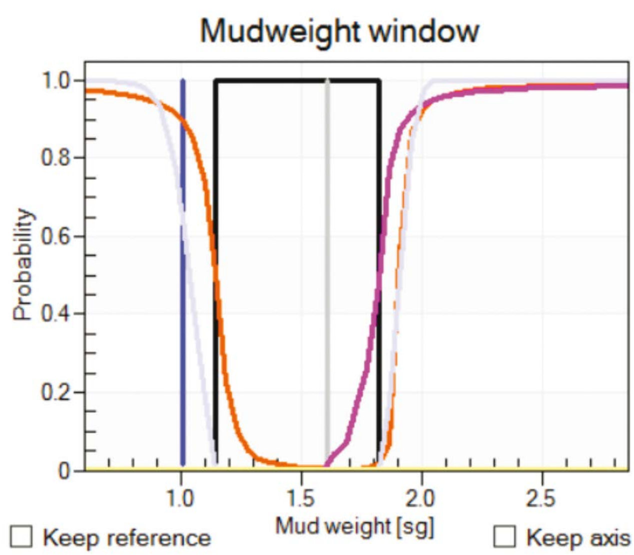

Figure 1. Mud weight window (solid black line) defined by 50 % probability of collapse and 50 % probability of fracturing. Blue curve is pore pressure gradient, orange curve is collapse gradient, pink curve is fracture gradient.

log files, where input properties are recorded from the logs at each given depth to produce a mud window in the form of collapse and fracture gradients vs depth along the well path.

The wellbore stability software already has an inbuilt uncertainty feature. This is visualized from variation of certain input parameters and yields probability for failure curves, where the mud window is defined for the 50 % probability of failure points (Fig. 1). Tensile failure and shear failure are calculated for all well pressure values, meaning that either failure mode could define either side of the mud window. In practice, shear failure dominates the lower side of the window, while tensile failure mostly explains the right-hand side of the window (hydraulic fracturing).

The user can also plot trends in the mud window as a function of input parameter change, re-calculating the window limits for the built-in range of the investigated parameter (Fig. 2).

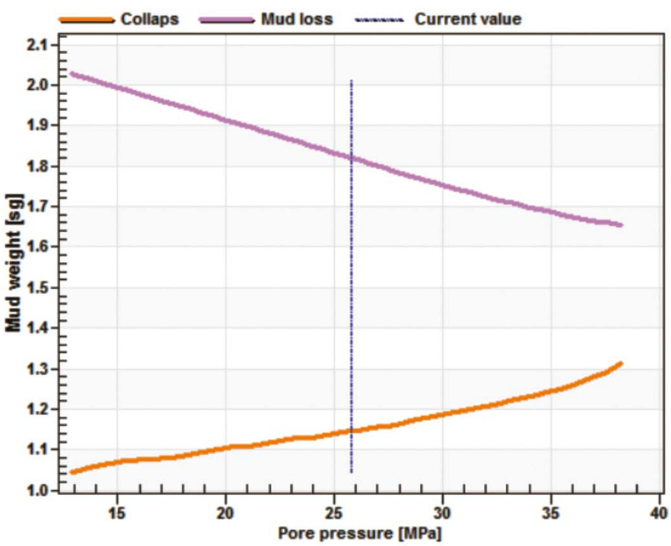

Figure 2. Sensitivity analysis (here, effect of pore pressure on mud window).

This feature is however not available in the log output mode, due to the computational penalty in redoing the calculations of the sensitivity analysis for all depths (Fig. 3).

The wellbore stability model described above has been chosen to be introduced in a real-time drilling advisory package, where the ambition is to combine pore pressure prediction, wellbore stability and hydraulic well control capabilities to help the drilling engineer make correct decisions while drilling (Rommetveit et al. 2010). The hydraulic module will predict ROP, torque and drag and associated risks for drill string incidents based on downhole sensor data collection. The pore pressure prediction module is based on another SINTEF software, which simulates compaction, erosion and uplift over geological times, taking into account basin-scale sealing compartments based on seismic imaged lithology and fault geometry (Lothe and Tømmerås 2006). this pore pressure prediction software runs many simulations in Monte-Carlo mode, where

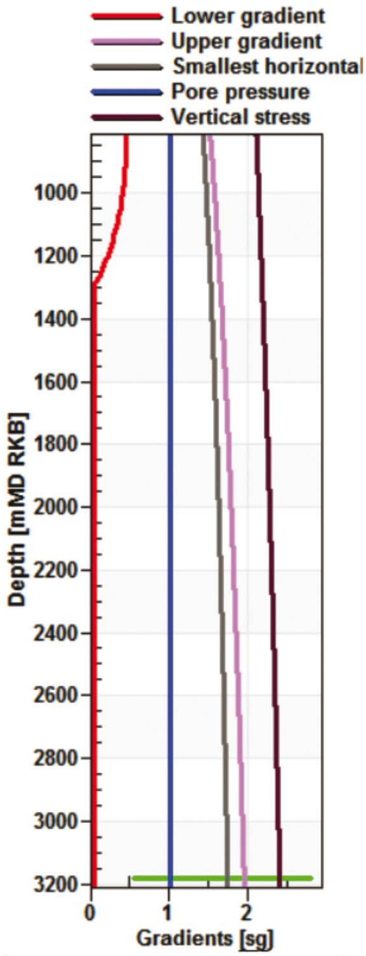

Figure 3. Log output mode. The mud window is shown as a function of depth. Red: shear failure, blue: pore pressure, grey: minimum horizontal stress, pink: tensile failure and brown: vertical stress.

fault transmissivity is altered and takes into account compaction induced pore pressure increase, compensated by leakage to neighboring compartments (controlled by evolving shale permeability including smectite-illite transition and hydraulic fracturing if relevant). The predicted pore pressure along the planned well trajectory is then passed on to the wellbore stability software to use in its mud window calculations.

This software package has been used in a number of studies with good results, even though direct real-time integration is still not completely achieved (Lothe et al. 2017). Since the pore pressure prediction comes with uncertainty in terms of the many Monte-Carlo realizations, it would make sense that the mud window prediction as a function of depth also would present to the driller the uncertainty accompanying the prediction. One way to achieve this ambition is simply to run 3 times the wellbore stability software, once for the minimum predicted pore pressure, once for the most likely and once for the maximum predicted pressure. However, other parameters influencing the accuracy of the window prediction are as difficult to assess such as elastic and mechanical properties, and in-situ stresses. Therefore, the approach described in this paper builds on a rigorous propagation of errors, however limiting itself to the principal sources of errors.

SOURCES OF UNCERTAINTY ESTIMATIONS

Different types and magnitudes of uncertainty enter mud weight window calculations, depending on the source of the input parameters. Information about variables such as stresses and pore pressure comes from regional exploration from basic geology and tectonics to detailed geophysical surveys, calibrated by direct measurements such as well tests in discrete points and depths of the surveyed domain. This information is rarely complete enough due to the scarcity of exploration wells and direct calibration tests in these wells. The use of geological and geomechanical large-scale models is necessary to generate hypotheses on the most probable value of these parameters in a continuous 3D domain.

Other sources of input parameters, especially for formation properties, are obtained through indirect in-well measurements. These are obtained via wireline logging tools measuring resistivity, neutron scattering, gamma ray emission and acoustic properties of the formations the well traverses, among others. Examples of formation properties detected by logging are porosity, permeability, pore fluid pressure, lithology, mechanical strength and stiffness. Regional or sometimes universal correlations relate the measured signal to a formation property, based on laboratory studies on retrieved core samples. Naturally, these correlations often consist of a cloud of points through which a regression exercise results in a mathematical function relating one or several measured quantities to a desired petrophysical or mechanical property.

Uncertainty on correlation-obtained properties depends on the type of function used; increasing the number of fit parameters will most of the time improve the regression correlation. However, the physical sense of the correlation often gets lost, especially for ranges of the calculated property outside the available data points. The SINTEF shale database includes more than 20 field cores from the North Sea and provides an important means of determining uncertainty in many shale parameters entering the mud window calculation. Most of the derived correlations are based on different laboratory tests on these field cores, such as strength, stiffness, porosity, permeability, acoustic velocities, fluid exposure tests, thermal effects etc. An example for shale strength correlation with acoustic velocity and with porosity is given in Fig. 4.

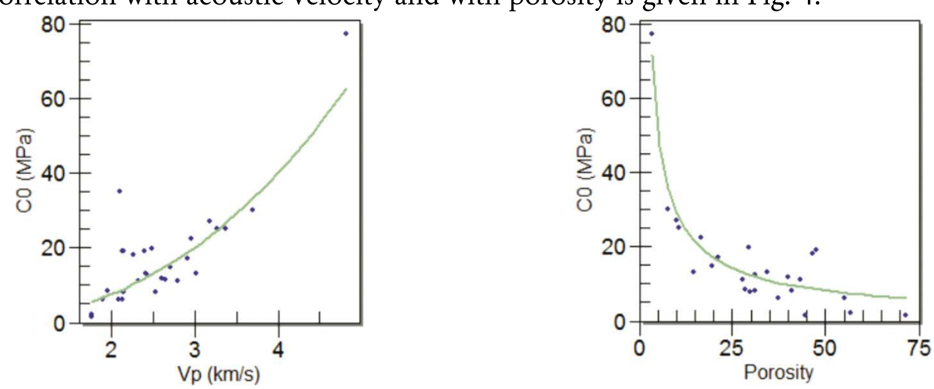

Figure 4. Correlations derived from the SINTEF shale test database. Left: shale strength as a function of ultrasonic velocity; right: strength as a function of porosity.

PROPAGATION OF ERROR CALCULATIONS

Given uncertainties in measured input or input evaluated from average values δ*xi*, the uncertainty for the calculated quantity δ*y* will be given by evaluating (to first order) the differential of the function used for the calculation, if it exists, where positive error values are insured by taking the square of the individual errors or their absolute values:

$$\delta y = \sqrt{\left(\frac{\partial y}{\partial x_i}\right)^2 \delta x_i^2} \qquad (1)$$

or

$$\delta y = \left|\frac{\partial y}{\partial x_i}\right| \delta x_i \qquad (2)$$

where the Einstein summation convention is assumed. A graphical illustration of the resulting uncertainty on a calculated function is seen in Fig. 5.

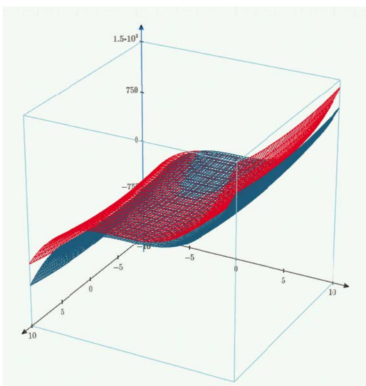

Figure 5. Uncertainty in a multivariate function resulting from input variable uncertainty. The red and blue surfaces frame the range of uncertainty in the function, varying along the input parameter axes (2 perpendicular variable axes in this case).

Uncertainty in borehole stresses: elastic case

The mud weight window is determined by the stress state at the borehole wall, comparing it to the strength of the rock in order to determine whether it will fail. Rock failure may occur in compression (shear) or tension, which is determined by using various model criteria (Fjær et al. 2008). A first step in error propagation analysis is to examine the variation in elastic stresses around a borehole, in terms of the calculated uncertainty. The elastic solution gives a conservative basis for estimating borehole failure in shear mode, since shear stress is proportional to the difference between two of the principal stresses and these diverge at the borehole wall. Note that for simplicity, we consider here isotropic horizontal stresses. However, it is seen from (Fig. 6), the calculated uncertainty itself decreases towards the borehole wall (borehole wall at 0 of x-axis). The uncertainty functions are calculated using the absolute value in the differential formulation, starting from the radial and tangential elastic stress distributions (equations (3) and (4)):

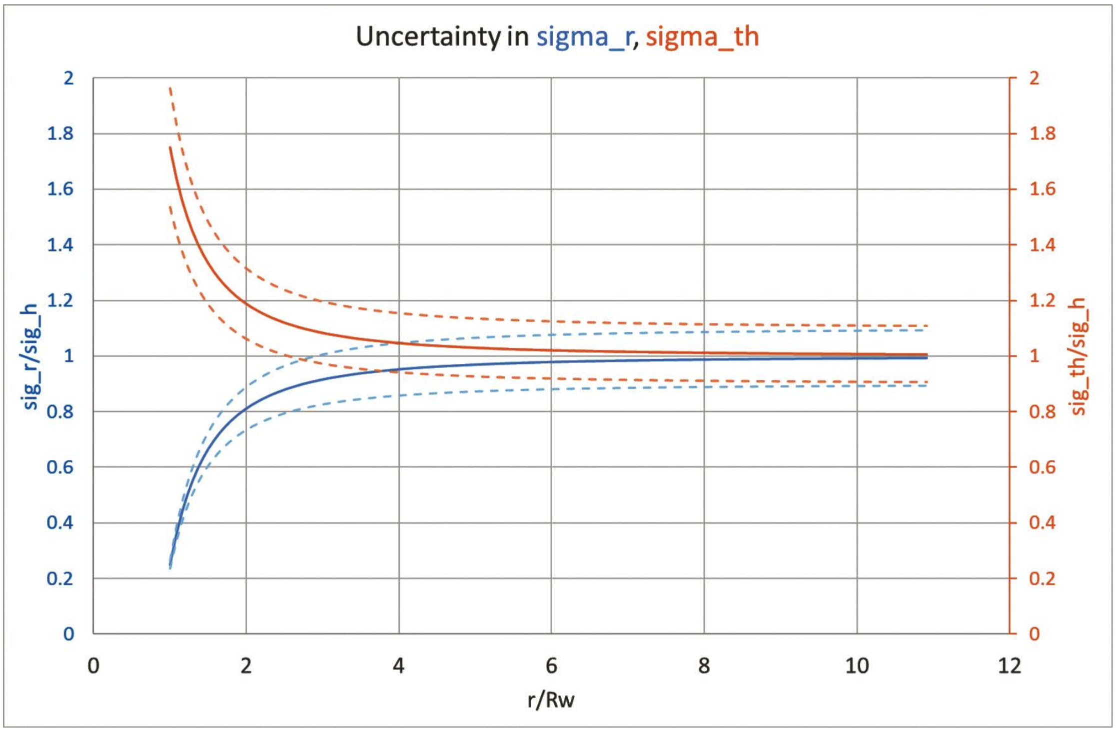

Figure 6. Radial elastic stress distribution around a vertical borehole (or in local coordinates along the wellbore axis). The dashed lines show the calculated uncertainty for chosen uncertainty values in the input parameters. sig_r: radial stress; sig_th: tangential stress; Rw: well radius and sig_h: in-situ horizontal stress.

$$\sigma_r(r) = \left(1 - \frac{Rw^2}{r^2}\right)\sigma_h + \frac{Rw^2}{r^2}p_W \tag{3}$$

$$\sigma_\theta(r) = \left(1 + \frac{Rw^2}{r^2}\right)\sigma_h - \frac{Rw^2}{r^2}p_W \tag{4}$$

where σ_r and σ_θ are the radial and tangential (or hoop) stress components, RW is the wellbore radius, σ_h is the far-field *in-situ* horizontal stress and p_w is the (mud) fluid pressure in the well. Taking the total differentials with respect to all uncertain parameters entering equations (3) and (4) yields the following uncertainty in total stresses, which makes the basis for the dashed lines in (Fig. 6):

$$d\sigma_r(r,\sigma_h) = \left|2(\sigma_h - p_W)\frac{Rw^2}{r^3}\right|dr + \left|1 - \frac{Rw^2}{r^2}\right|d\sigma_h \tag{5}$$

$$d\sigma_\theta(r,\sigma_h) = \left|2(p_W - \sigma_h)\frac{Rw^2}{r^3}\right|dr + \left|1 + \frac{Rw^2}{r^2}\right|d\sigma_h \tag{6}$$

Uncertainty in borehole stresses: Mohr-Coulomb case

Plasticity can be introduced using a failure criterion, with the effect of mitigating the principal stress divergence at the borehole wall, reducing the shear stress in the plastified zone. This mitigation is shown for the Mohr-Coulomb criterion, with the (effective) stress distribution around the wellbore plotted in (Fig. 7).

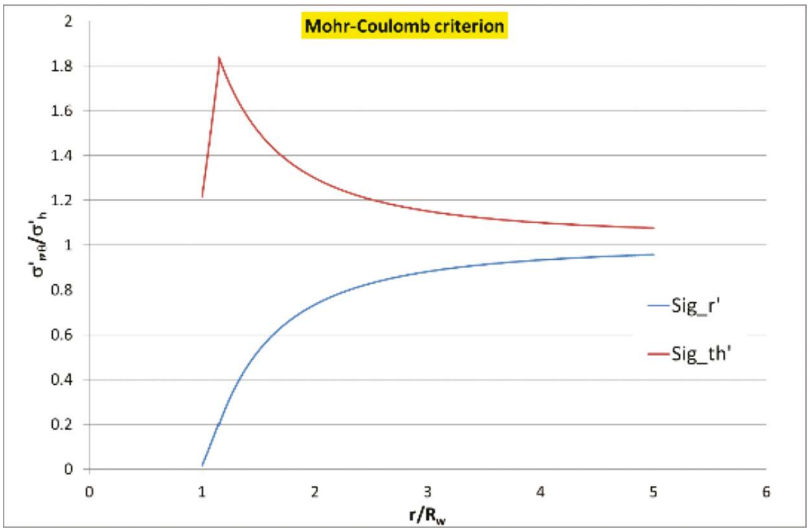

Figure 7. Attenuation of stress anisotropy in the vicinity of the well when taking into account plastic yield (for high enough far-field stress or low enough well pressure) using the Mohr-Coulomb criterion. Sig_r': radial effective stress; Sig_th': tangential effective stress; Rw: well radius and σh': *in-situ* horizontal effective stress.

The same approach as before is used to calculate the stress uncertainty distribution. Following (Fjær *et al.* 2008), the stresses are given in the plastified zone as:

$$\sigma_r(r) = \left(p_W + \frac{C_0'}{k'-1}\right)\left(\frac{r}{R_W}\right)^{k'-1} - \frac{C_0'}{k'-1} \qquad (7)$$

$$\sigma_\theta'(r) = C_0' + k'\sigma_r' \qquad (8)$$

$$k' = \tan^2\beta' \qquad (9)$$

where C0 is the uniaxial compressive strength of the rock, β is the failure angle and prime variables denote post-peak parameters (residual strength, cohesion and friction angle). The extent of the plastified zone is found by equating the stresses at its boundary, denoted by the plastic radius Rp:

$$\frac{R_p}{R_W} = \left[\frac{2\sigma_h + (1-k)\mathcal{A} + (1+k)\mathcal{A}'}{(1+k)(p_W + \mathcal{A}')}\right]^{\frac{1}{k'-1}} \qquad (10)$$

$$\mathcal{A} = \frac{C_0}{(k-1)} \qquad (11)$$

The plastic radius is manifested in (Fig. 7) as the sharp turn from increasing tangential stress towards the well, to decreasing values in the plastic zone. The corresponding total differentials are then calculated to find the uncertainty function of (Fig. 8):

$$d\sigma_r = \left|\left(\frac{r}{R_W}\right)^{k-2}\frac{(k-1)}{R_W}\left(p_W + \frac{C_0}{k-1}\right)\right| dr + \left|\frac{1}{k-1}\left[\left(\frac{r}{R_W}\right)^{k-1} - 1\right]\right| dC_0 + \left| C_0 \frac{1-\left(\frac{r}{R_W}\right)^{k-1}}{(k-1)^2} + \ln\left(\frac{r}{R_W}\right) \cdot \left(\frac{r}{R_W}\right)^{k-1} \cdot \frac{C_0 - p_W(1-k)}{k-1}\right| \tan\beta \cdot (1 + \tan^2\beta) d\phi \qquad (12)$$

with ϕ being the friction angle.

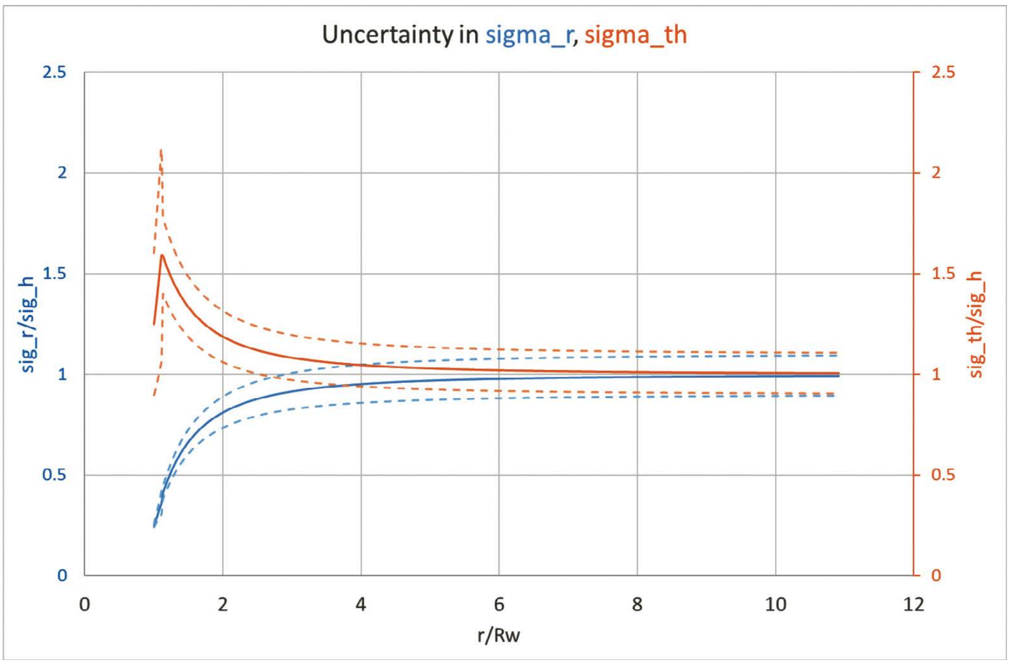

Figure 8. Stress anisotropy in the vicinity of the well using the Mohr-Coulomb criterion, with associated uncertainty. Sig_r: radial stress; Sig_th: tangential stress and Rw: well radius.

The radial stress uncertainty vanishes again towards the borehole, while the tangential stress uncertainty does not.

Uncertainty in fracture and collapse gradients

Expressing the stresses in terms of the well pressure, *pw*, and incorporating shear failure on the one hand, and tensile failure criteria, on the other, gives the lower and upper mud weight limits, respectively. Adding the propagation of error calculations described above, one finally gets to an expression giving the uncertainty on the mud weight window. Equation (13) gives the total differential calculated for the collapse and frac limits:

$$dp_{W,\mathrm{col}} = \left|1 - \frac{2}{\tan^2\beta+1}\right| dp_f + \left|\frac{3}{\tan^2\beta+1}\right| d\sigma_H + \left|\frac{-1}{\tan^2\beta+1}\right| d\sigma_h + \left|-\frac{1}{\tan^2\beta+1}\right| dC_0 + \left|\frac{\cos(\phi)\cdot[C_0-3\sigma_H+\sigma_h+2p_f]}{2}\right| d\phi$$

$$dp_{W,\mathrm{frac}} = 3d\sigma_h + d\sigma_H + dp_f + dT_0 \qquad (13)$$

where *pf* is the formation pore pressure, σ_H is the major horizontal stress and T0 is the shale tensile strength. Note that we take here the general case where the horizontal stresses are not isotropic but only consider the case of a vertical well, with tangiential stress at the borehole

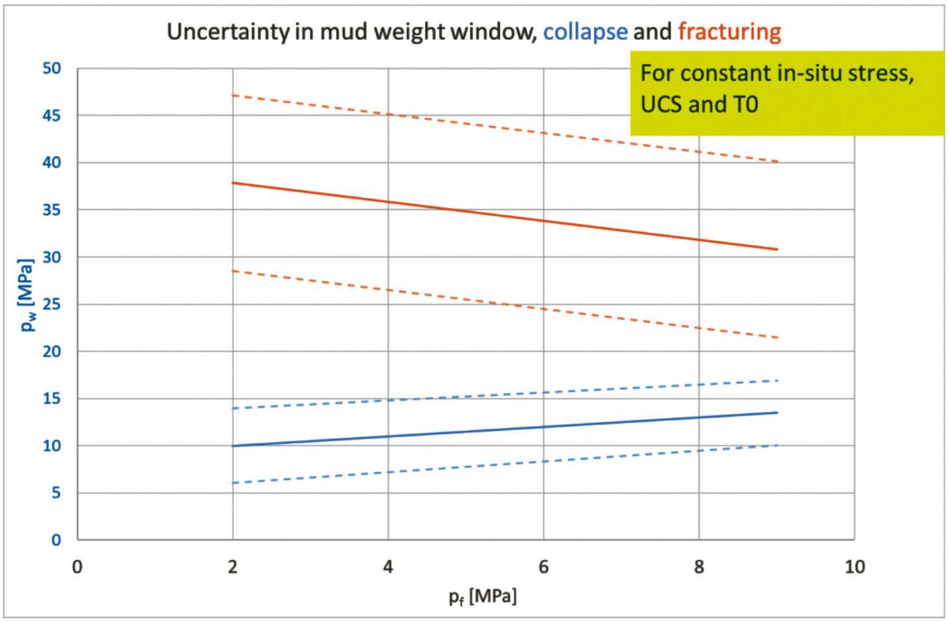

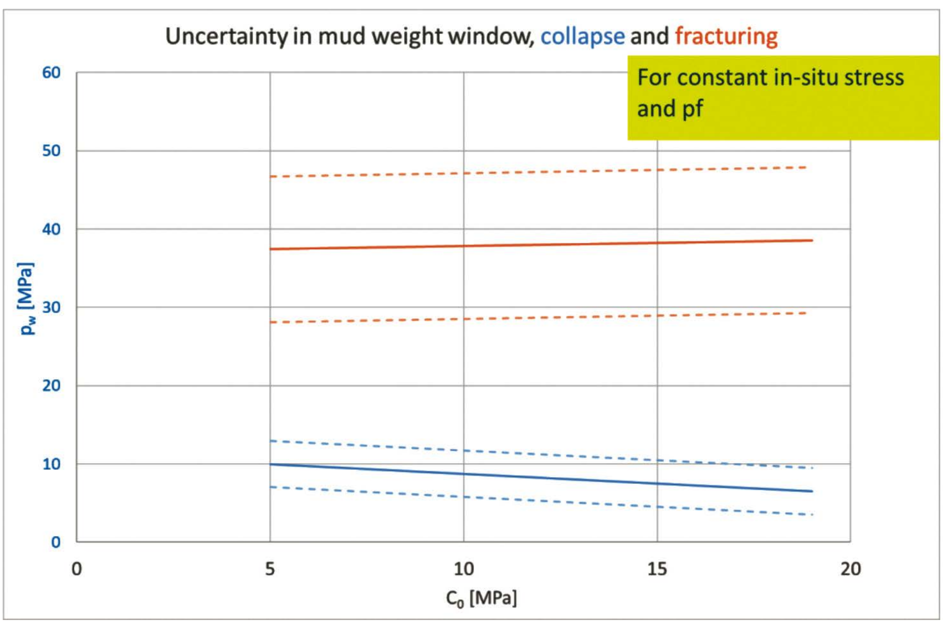

Figure 9. Two examples of mud window uncertainty calculations plotted as a function of in-situ pore pressure (top) and as a function of uniaxial compressive strength (bottom).

being the major principal stress. The uncertainty in pore pressure dpf will come from the Pressim pre-drill simulation and eventually be replaced in real-time with reduced values as production logs are taken. The uncertainty in stresses will be obtained from regional trends calibrated with XLOTs for the minor horizontal stress. The major horizontal stress is more difficult to estimate and may in principle vary between the minimum horizontal stress and the vertical stress, assuming a normal fault regime at depth. Near existing faults in the field, this stress stata assumption may not be correct, as a rotation of the local stress tensor has probably occurred during faulting. The uncertainties in cohesion and friction angle are obtained from regional correlations and/or laboratory data on similar formations. Two examples of calculated mud window uncertainties are given in (Fig. 9). Note that the uncertainty on the fracturing side is larger than on the collapse side; however, all input uncertainties are taken as independent of each other, which is a conservative approach. More realistic calculations would give less error, as will be seen next.

The examples given above apply to a vertical well; generalisation to deviated wells is done by rotating the in-situ stress field to coincide with the well's axis, then exploring all angles around the well's cross section to find the maximum principal stress difference orientation.

USE OF COVARIANCE ANALYSIS TO REDUCE UNCERTAINTY

The additive propagation of uncertainties can often generate a very careful and conservative estimate of total uncertainty, as exemplified in (Fig. 9). A priori fundamental knowledge and field experience captured in (regional) empirical correlations, imply that some of the uncertainties entering the calculation are not independent variables. To explore the dependence between these uncertainty variables, correlation matrices are calculated, from which a correlation matrix can be evaluated. This is in turn re-injected in the error propagation formula (eq. (1)), generalizing it to include cross-terms:

$$\delta y = \sqrt{\left(\frac{\partial y}{\partial x_i}\right)^2 \delta x_i^2 + 2r_{x_i x_j}\left(\frac{\partial y}{\partial x_i}\right)\left(\frac{\partial y}{\partial x_j}\right)\delta x_i \delta x_j} \qquad (14)$$

where rxi,xj denotes the components of the correlation matrix. These components vary between -1, completely anticorrelated, to +1, completely correlated. In eq. (1) the assumption is therefore that all uncertainties are completely uncorrelated. This is clearly not the case when one for example expects that mechanical strength will correlate with stiffness and be anticorrelated with Poisson's ratio and permeability, at least in the North Sea.

Uncertainty variation between calibration wells

The following example illustrates the advantage of a priori knowledge and more realistic uncertainty propagation using existing wells as calibration points. (Fig. 10) shows a table where key properties needed to calculate the shear failure or collapse side of the mud window are shown; the mud window needs to be calculated for new wells placed between two existing wells. The different parameters are evaluated with varying uncertainty, decreasing at the calibration wells. However, the uncertainty is never completely reduced at the calibration points, since many parameters are still not measured directly at these calibration points (which would in theory be reduced to just the experimental measurement error). For simplicity and illustration purposes, the example treats only one depth and uses the more common Mohr-Coulomb calculation already presented above (vertical well).

	Well 1				Well 2
Pore pressure p_f [MPa]	23	22	21	19	17
Minimum horizontal stress σ_h [MPa]	30	28	27	26	25
Maximum horizontal stress σ_H [MPa]	31.5	29.4	28.35	27.3	26.25
Uniaxial compressive strength C_0 [MPa]	9	8.25	7.5	6.75	6
Friction angle ϕ [-]	32	33	35	44	46
dp_f [MPa]	0.5	1	2	0.75	0.25
$d\sigma_h$ [MPa]	1	2	3	2	1
dC_0 [MPa]	2	4	5	3	2
$d\phi$ [-]	1	2	4	3	2

Figure 10. Example of parameter evaluation in order to calculate the variation of the collapse limit for new wells, calibrated on existing wells. dpf, dσh, dC_0 and dϕ – uncertainty in formation pore pressure, minimum horizontal stress, unconfined compressive strength and friction angle, respectively.

The next step is to calculate the correlation matrix in order to evaluate the propagated uncertainty using Eq. (14). Since significant a priori knowledge has been used in evaluating the four parameters, it is expected that the cross terms will not be zero and may potentially reduce the uncertainty as opposed to a random pick of the variables. The correlation matrix is obtained from the variance-covariance matrix:

$$corr(\boldsymbol{X}) = \left(diag(\boldsymbol{V})\right)^{-\frac{1}{2}}\boldsymbol{V}\left(diag(\boldsymbol{V})\right)^{-\frac{1}{2}} \quad (15)$$

with the variance-covariance matrix calculated from:

$$\boldsymbol{V} = cov(\boldsymbol{X}) = E\left[\left(\boldsymbol{X} - E(\boldsymbol{X})\right)\left(\boldsymbol{X} - E(\boldsymbol{X})\right)^{T}\right] \quad (16)$$

where E denotes the expected value of a vector. The correlation matrix calculated for the table in (Fig. 10) is shown in (Fig. 11); (Fig. 12) shows the obtained collapse limit with uncertainty between the two calibrating wells. In (Fig. 12), one can appreciate the reduction in uncertainty evaluation between the conservative use of Eq. (1) as opposed to taking advantage of the knowledge-based correlation between the variables in (Fig. 10).

	pf	sigh	sigH	C0	phi
pf	1	0.949812	0.949812	0.761577	-0.97132
sigh	0.949812	1	1	0.986394	-0.89713
sigH	0.949812	1	1	0.986394	-0.89713
C0	0.761577	0.986394	0.986394	1	-0.94589
phi	-0.97132	-0.89713	-0.89713	-0.94589	1

Figure 11. Correlation matrix corresponding to the variables in the table of (Fig. 10).

	pf	sigh	sigmaH	T0
pf	1	0.949812	0.949812	0.216149
sigh	0.949812	1	1	0.365739
sigmaH	0.949812	1	1	0.365739
T0	0.216149	0.365739	0.365739	1

Figure 12. Variation of estimated collapse limit in a prospected area between two existing wells. The figure illustrates the uncertainty reduction obtained by calculating the correlation matrix and adding the cross terms in Eq. (14) – dashed lines – as compared to assuming independent errors as in Eq. (1) – dotted lines.

Next, the upper limit is addressed. (Fig. 13) shows the estimated parameter uncertainties. Note that we assume complete positive correlation between minor and maximum horizontal stresses, with the same error away from the calibrating wells. This is due to the likelihood that the 2 calibrating wells would be chosen in the same basin or geological setting, implying the same tectonic stress regime. Thus, we assume here that a 5% difference exists between the 2 horizontal stress components, and any departure from this ratio will be covered by the increasing uncertainty with distance from the wells. (Fig. 14) shows the obtained correlation matrix. The obtained combined uncertainty for the fracturing limit is shown in (Fig. 15), where the effect of prior knowledge on parameter dependence has a pronounced influence on uncertainty magnitude. Finally, the obtained mud weight window is shown in (Fig. 16), combining lower and upper limit, with uncertainty estimated upon a priori trends. Note that this window only represents one depth; in practice, the exercise would be repeated at several depths along the planned well paths. Again, this entails rotating the stress tensor as needed with changing path inclination and azimuth with respect to the principal horizontal stresses.

	pf	sigh	sigmaH	T0
pf	1	0.949812	0.949812	0.216149
sigh	0.949812	1	1	0.365739
sigmaH	0.949812	1	1	0.365739
T0	0.216149	0.365739	0.365739	1

Figure 13. Example of parameter evaluation in order to calculate the variation of the fracturing limit for new wells, calibrated on existing wells. d_{pf}, $d\sigma_h$, $d\sigma_H$ and dT_0 – uncertainty in formation pore pressure, minimum and maximum horizontal stress and tensile strength, respectively.

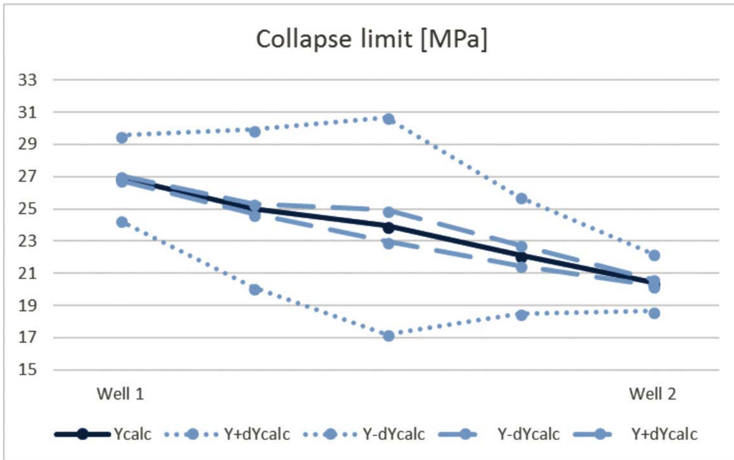

Figure 14. Correlation matrix corresponding to the variables in the table of Fig. 13.

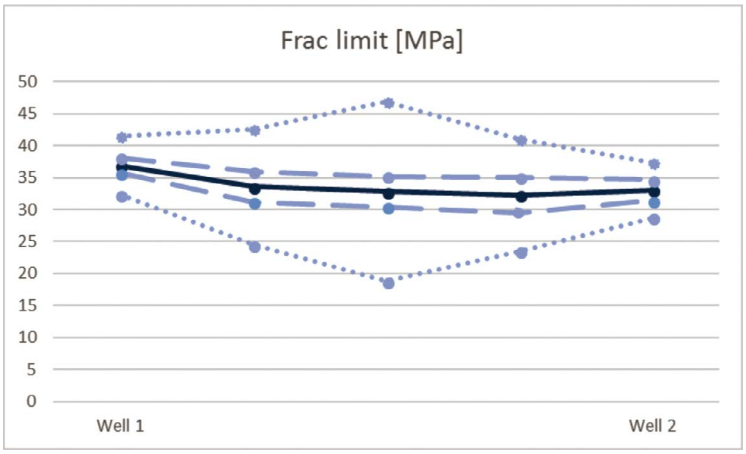

Figure 15. Variation of estimated tensile or fracturing limit in a prospected area between two existing wells. The figure illustrates the uncertainty reduction obtained by calculating the correlation matrix and adding the cross terms in Eq. (14) – dashed lines – as compared to assuming independent errors as in Eq. (1) – dotted lines.

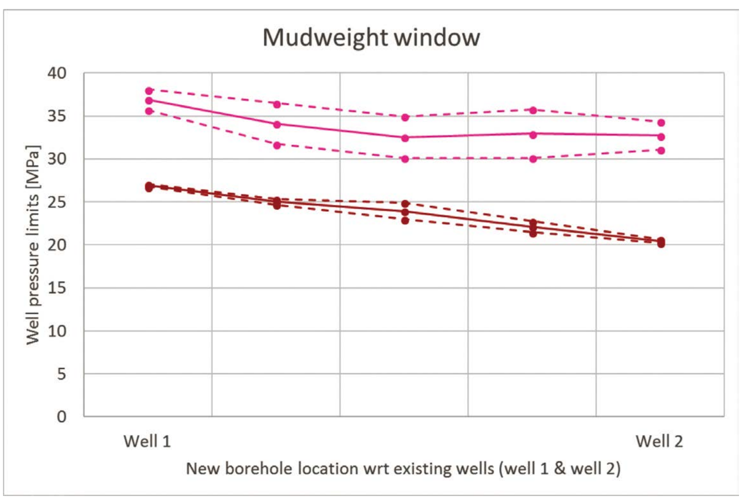

Figure 16. Mud weight window for planned vertical wells at a given depth, between two existing wells, together with prediction uncertainty.

Uncertainty update while drilling

The effect of increased knowledge on uncertainty can also be experienced while drilling, assuming that updates are made available through acquired wireline logs or other downhole sensors. A similar exercise as presented above can be made to illustrate the potential for implementation of the method into an automated drilling tool, where an updated mud window can be shown to the drilling engineer in quasi real-time, together with updated uncertainty. The simplest way to proceed is to take the same number of evaluation points as before, but turn the axes by 90°, such that a window as a function of 5 discrete depths is obtained.

The available a priori input will be slightly different: instead of having two calibration points, general knowledge about depth trends for the parameters will be used. Thus, it is expected that material strength most likely increases with depth, as well as all components of in-situ stress; pore pressure usually also increases with depth, however trapping of fluid in low permeability formations often leads to over-pressured zones. This means that pore pressure is not expected to be a monotonous function of depth; this will also be to some extent reflected on the minimum horizontal stress. Again, an educated guess at what values to expect along the well path is shown together with uncertainty in the table of (Fig. 17). For simplicity, only the upper limit is calculated. The frac limit and uncertainties are presented in (Fig. 18).

In (Fig. 19), the assumption is that the drill bit has progressed to the depth of the second column, confirming the values from the pre-drill model. Note again, that due to mostly indirect measurements through log correlations, the uncertainty is reduced but not to purely experimental measurement error. The other columns, representing deeper layers, also benefit from confirmed knowledge as a better, new prediction of the subsurface is made. This is confirmed by the reduced total uncertainty, also ahead of the bit (Fig. 20).

	Depth 1				Depth 2
p_f [MPa]	17	18	19	22	21
σ_h [MPa]	25	27	28	29	29
σ_H [MPa]	26	28	29	29	30
T_0 [MPa]	1.33	0.77	0.93	1.06	0.82
dp_f [MPa]	0.5	0.75	0.75	0.75	0.75
$d\sigma_h$ [MPa]	0.5	1	1	1	1
$d\sigma_H$ [MPa]	0.75	1	1	1	1
dT_0 [MPa]	0.07	0.04	0.05	0.05	0.04

Figure 17. Example of parameter evaluation in order to calculate the variation of the fracturing limit as a function of depth along a vertical well path. dpf, $d\sigma_h$, $d\sigma_H$ and dT_0 – uncertainty in formation pore pressure, minimum and maximum horizontal stress and tensile strength, respectively.

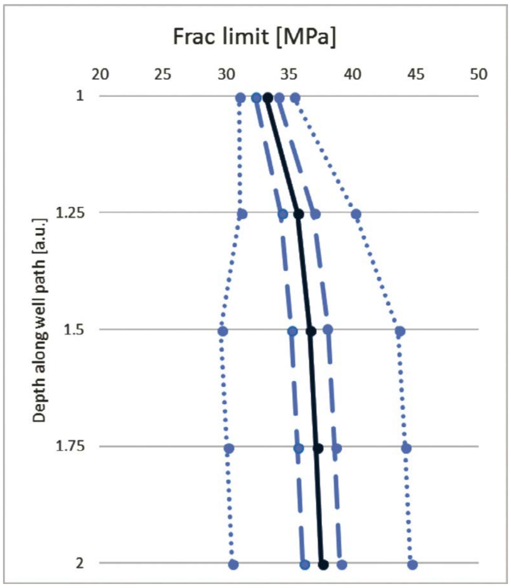

Figure 18. Variation of estimated tensile or fracturing limit as a function of depth for a planned vertical well. The figure illustrates the uncertainty reduction obtained by calculating the correlation matrix and adding the cross terms in Eq. (14) – dashed lines – as compared to assuming independent errors as in Eq. (1) – dotted lines.

	Depth 1				Depth 2
p_f [MPa]	17	18	23	22	21
σ_h [MPa]	25	27	30	29	29
σ_H [MPa]	26	28	31	30	30
T_0 [MPa]	1.33	0.77	0.93	1.06	0.82
dp_f [MPa]	0.1	0.1	0.3	0.5	0.75
$d\sigma_h$ [MPa]	0.15	0.15	0.5	0.75	1
$d\sigma_H$ [MPa]	0.15	0.15	0.5	0.75	1
dT_0 [MPa]	0.02	0.04	0.06	0.08	0.05

Figure 19. Example of parameter evaluation in order to calculate the variation of the fracturing limit as a function of depth along a vertical well path. The drill bit has reached the depth of the second column (green numbers show confirmed values).

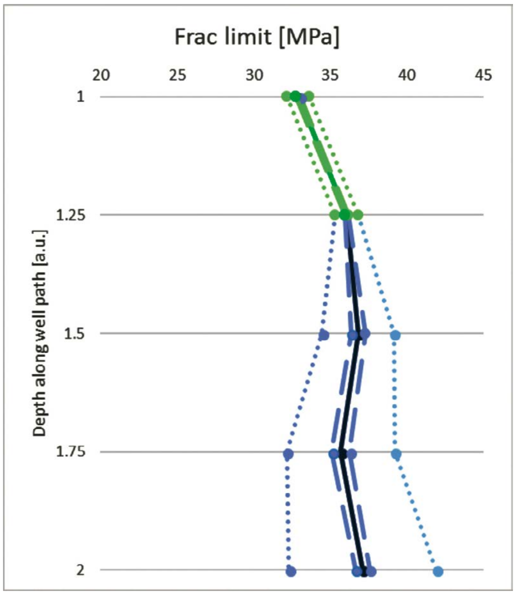

Figure 20. Reduction of the estimated fracturing limit uncertainty as a function of depth for a planned vertical well. The upper green part of the plot shows the already drilled part of the well, with its obviously reduced uncertainty.

DISCUSSION & CONCLUSION

The mud weight window is the most important predictive tool for the drilling engineer. A reliable prediction will facilitate problem-free drilling to target, minimizing the time and hence the cost needed to reach the reservoir. Consequently, having an erroneous mud window may cause serious HSE issues such as gas kicks or large cost increases for the whole drilling program by prolonging the time needed to reach target depth. Planning for the wrong mud composition and density can lead to either stuck pipe or mud loss, both incidents immobilizing the drilling bit and necessitating costly workover operations. Pulling out of hole and back in may induce pressure surges and drops, further compromising the well's stability. Having a proper indication of the mud window for the whole drilling interval allows the drillers to plan an optimal mud density program; ideally, there should be minimal need for frequent density adjustments and mud composition changes, which bring up the costs due to more complex logistics and often more costly fluid types. This optimization will often bring the driller to briefly touch either window limit; having the uncertainty linked to the prediction displayed as proposed in this paper will certainly help make a more informed decision, based on a more quantitative risk assessment.

The definition itself of the mud window differs from operator to operator; the most conservative definition will be from the largest value of either collapse limit or pore pressure, to the minimum horizontal stress. Should the pore pressure be higher than the collapse limit, remaining above the pore pressure ensures that the well is at all times drilled in over-balanced conditions, to avoid the risk of fluid influx. Staying below the minimum horizontal stress takes into account the risk of drilling into a naturally fractured formation, where exceeding the minimum horizontal stress may open enough the fracture to cause mud losses. Having the uncertainty displayed again makes taking risks such as going for managed pressure drilling or exceeding the minimum horizontal stress easier to handle.

Combining a display of the uncertainty with frequent updates while drilling simplifies greatly the driller's ability to react ahead of unforeseen incidents, where changes made in time to the drilling fluid program may avoid non-productive time necessary to put the drilling operation on track again. The updates will result, as has been seen in the simple example above, in increased confidence in the mud window, which will either be updated with new estimates or have the pre-drill uncertainty narrowed down.

Propagation of errors is a simple way to quantify the confidence level in predicted quantities involving calculations with several different input variables. The default formulation of error propagation is for all practical purposes a very conservative estimate, more suitable for evaluating direct measurement and systematic errors in relatively simple cases. When dealing with many different sources of input variables, with the uncertainty amplified by the needed use of indirect evaluation methods such as correlations, the estimated errors become rapidly too large to be manageable. Instead of helping understand the confidence on the calculated estimates, too large an uncertainty will strip the calculation of any quantitative application. Selecting appropriate calibration points for the mud window calculations, together with careful use of a priori choice of estimated trends, helps reduce significantly the uncertainty through the use of correlated data, wherever possible. Finally, it seems for the authors that presenting simple 2-component mud windows, with lower and higher limit and their uncertainty is more useful than the current practice with many gradients displayed but without any uncertainty.

Acknowledgements

This work was performed in the framework of the KPN (competence-building for the industry) project: "Reduced uncertainty in overpressures and drilling window prediction ahead of the bit (PressureAhead)" #255418/E30 funded by The Research Council of Norway and the DrillWell SFI Centre with support of AkerBP, Wintershall, ConocoPhillips and Statoil.

CITED REFERENCES

Bratli, R. K. and R. Risnes,1981. "Stability and Failure of Sand Arches."

Cerasi, P., A. M. Stroisz, L. E. Walle and A. Lavrov, 2014, "Laboratory testing of shale rock specimens to assess thermal fracturing risk in caprock surrounding injection wells", 48th US Rock Mechanics/Geomechanics Symposium Proceedings, American Rock Mechanics Association (ARMA): 6.

Fjar, E., R. M. Holt, A. M. Raaen, R. Risnes and P. Horsrud, 2008, "Petroleum Related Rock Mechanics", Elsevier Science.

Fjær, E., R. M. Holt, P. Horsrud, A. M. Raaen and R. Risnes, 2008, "Chapter 9 Stability during drilling. Petroleum Related Rock Mechanics", R. M. H. P. H. A. M. R. E. Fjær and R. Risnes, Elsevier. Volume 53: 309-339.

Fjær, E., R. M. Holt, O.-M. Nes and E. F. Sønstebø, 2002, "Mud Chemistry Effects on Time-Delayed Borehole Stability Problems in Shales", Society of Petroleum Engineers.

Horsrud, P., B. Bostrom, E. Sonstebo and R. Holt, 1998, "Interaction between shale and water-based drilling fluids: laboratory exposure tests give new insight into mechanisms and field consequences of KCl contents", SPE Annual Technical Conference and Exhibition, Society of Petroleum Engineers.

Horsrud, P., E. F. SØnstebØ and R. BØe, 1998, "Mechanical and petrophysical properties of North Sea shales", International Journal of Rock Mechanics and Mining Sciences 35(8): 1009-1020.

Karaborni, S., B. Smit, W. Heidug, J. Urai and E. Van Oort, 1996, "The swelling of clays: molecular simulations of the hydration of montmorillonite", Science 271(5252): 1102-1104.

Lavrov, A. and P. Cerasi, 2013, "Numerical modeling of tensile thermal stresses in rock around a cased well caused by injection of a cold fluid", 47th US Rock Mechanics/Geomechanics Symposium Proceedings, American Rock Mechanics Association (ARMA): 8.

Lavrov, A. and J. Tronvoll, 2006, "Numerical analysis of radial flow in a natural fracture: applications in drilling performance and reservoir characterization", Abu Dhabi International Petroleum Exhibition and Conference, Society of Petroleum Engineers.

Lomba, R. F., M. Chenevert and M. M. Sharma, 2000, "The ion-selective membrane behavior of native shales", Journal of Petroleum Science and Engineering 25(1-2): 9-23.

Lothe, A., P. Cerasi, S. Haavardstein and K. Bjorkvoll, 2017, "Workflow for Uncertainty Modelling of Pore Pressure and Mud Weight Window ahead of Bit-Example of Pre-drill Results from the North Sea", First EAGE Workshop on Pore Pressure Prediction.

Lothe, A. and A. Tømmerås, 2006, "Stochastic Monte-Carlo simulations of overpressure probability distribution in the Halten Terrace area", AAPG Conference, Perth.

Nes, O.-M., R. Boe, E. F. Sonstebo, K. Gran, S. Wold, A. Saasen and A. Fjogstad, 2012, "Borehole Instability in Tertiary Shales in the Norwegian North Sea", Society of Petroleum Engineers.

Nes, O. M., A. Brenna, K. Gran and A. Saasen, 2013, "Borehole Shale Stability Analysis to Facilitate Successful Drilling of a Horizontal Well in the North Sea", 47th U.S. Rock Mechanics/Geomechanics Symposium. San Francisco, California, American Rock Mechanics Association.

Rommetveit, R., K. S. Bjorkevoll, P. R. Cerasi, S. T. Havardstein, M. Fjeldheim, H. M. Helset, S. I. Odegard and C. Nordstrand, 2010, "Real Time Integration of ECD, Temperature, Well Stability and Geo/Pore Pressure Simulations during drilling a challenging HPHT well", Society of Petroleum Engineers.

Torsaeter, M., P. E. Vullum and O.-M. Nes, 2012, "Nanostructure vs. Macroscopic properties of mancos shale", SPE Canadian Unconventional Resources Conference, Society of Petroleum Engineers.

Torsæter, M. and P. Cerasi, 2015, "Mud-Weight Control During Arctic Drilling Operations", Arctic Technology Conference. Copenhagen.